Electric Power Systems Research 199 (2021) 107370

Contents lists available at ScienceDirect

Electric Power Systems Research

journal homepage: www.elsevier.com/locate/epsr

Measurement and assessment of corona current density for HVDC bundle conductors by FDM integrated with full multigrid technique

Mohamed A. Abouelatta [a], Sayed A. Ward [a,b], Ahmad M. Sayed [a], Karar Mahmoud [c,d], Matti Lehtonen [d], Mohamed M.F. Darwish [a,d,*]

[a] Department of Electrical Engineering, Faculty of Engineering at Shoubra, Benha University, 11629 Cairo, Egypt
[b] Faculty of Engineering, Delta University for Science and Technology, 11152 Mansoura, Egypt
[c] Department of Electrical Engineering, Faculty of Engineering, Aswan University, 81542 Aswan, Egypt
[d] Department of Electrical Engineering and Automation, School of Electrical Engineering, Aalto University, FI-00076 Espoo, Finland

ARTICLE INFO

Keywords:
HVDC Bundle transmission
Finite difference method
Full multigrid method
Corona losses

ABSTRACT

This paper presents an intensive measurement and analysis of monopolar ionized fields in bundled high voltage direct current (HVDC) conductors using the finite difference method based on the full multigrid technique. The positive feature of this study is that it considers the comprehensive representation of the bundle conductor, unlike the existing studies that approximate the bundle conductor with an equivalent conductor radius. Firstly, the proposed method is compared with previous experimental results. Secondly, a flexible laboratory model for the bundled HVDC conductors is constructed. Thirdly, the laboratory model is exploited to validate the numerically computed current density distribution on the ground plane and corona current for different bundles' numbers and different distances between bundles. Bundles of one, two, and four conductors are adopted in the experimental setup. For the same applied voltage, the results verified that the corona current decreases by increasing the bundles' number and/or minimizing the spacing between bundles. Consequently, the obtained results confirmed that corona power losses can be minimized, without needing the traditional procedures that involve increasing either the conductor radius or its height above the ground. The results of the proposed numerical approach concurred well with the present and past laboratory results.

1. Introduction

With the colossal increment in power transmitted over long distances, high voltage direct current (HVDC) transmission has turned out to be emulative, and numerous HVDC transmission lines are developed everywhere throughout the world [1-4]. HVDC transmission systems are run exceeding the corona onset voltage, which may lead to several biological effects, audible noise, radio and TV interference, power losses, and the insulation systems deterioration [5-8]. This has shaped a developing concern for the study of corona losses on HVDC transmission lines. Conductor bundling is implemented in HVDC transmission lines to enhance their corona rate without needing unreasonably huge conductors [9]. Bundling is mainly used to reduce the electric field at the sub conductors' surface, which will bring about increasing the corona onset voltage, reducing the corona power losses, television, and radio interference, and audible noise [10-13].

Investigation of the corona fields resulting from monopolar stressed electrodes is significant in the manufacturing stage of HVDC transmission lines [14, 15]. The existing corona problem in the HVDC transmission systems is of a non-linear nature, so solving the fields associated with corona exactly is extremely difficult. Several attempts are carried out to develop numerical techniques, including the finite element method (FEM) [16-25], the boundary element method (BEM) [26, 27], the charge simulation method (CSM) [28-31], and hybrid techniques [1, 9], to estimate the corona power losses on monopolar HVDC transmission systems. According to the authors' knowledge, limited attempts are implemented to solve the corona problem on bundled HVDC conductors [30-38]; However, none of them applied the numerical finite difference method (FDM) combined with the full multigrid method (FMG), which is the main focus of this work.

The FDM is a numerical procedure that approximates the equations by disregarding the terms of a higher order, which may result in a

* Corresponding author.
E-mail addresses: moh_an1@yahoo.com (M.A. Abouelatta), drsayedw@yahoo.com (S.A. Ward), ahmad_m_omar@yahoo.com (A.M. Sayed), karar.mostafa@aalto.fi (K. Mahmoud), matti.lehtonen@aalto.fi (M. Lehtonen), mohamed.m.darwish@aalto.fi (M.M.F. Darwish).

https://doi.org/10.1016/j.epsr.2021.107370
Received 25 November 2020; Received in revised form 1 February 2021; Accepted 12 May 2021
Available online 26 May 2021

considerable truncation error to be lessened via finer grids. However, if the iterative method is not chosen well, it will be time-wasting relative to computation. The convergence rate of the most traditional iterative techniques is poor regarding the finer grids. Therefore, different iterative strategies should be applied to implement fine grids without experiencing the high computational period. Using the multigrid method, this issue can be treated well and it improves dramatically the rate of convergence of the traditional iterative techniques [39-43]. The multigrid principle transforms the fine mesh into a coarser mesh. The traditional iterative techniques work on the coarse meshes and then using the transfer operators of the grid, the obtained results are implemented as an enhanced initial estimation for finer meshes [39,44].

To address the limitations of the existing above-mentioned studies, this work is aiming to measure and analysis of monopolar ionized fields in bundled HVDC transmission line systems using a proposed FDM integrated with the FMG iterative solver. Among the different schemes of the multigrid technique, the full multigrid variant is implemented as an iterative strategy for the FDM to deal with the corona discharge issue, especially on fine grid computational domains. In the present analysis, Poisson and current continuity equations for the monopolar bundled HVDC transmission systems are solved using the FDM integrated with the FMG to deal with finer meshes without facing a high execution period. To show the validity of the proposed method, the proposed numerical approach (FDM-FMG) concurred well with past laboratory results. Besides, an experimental setup is constructed to measure the corona discharge of the HVDC bundled transmission line. Using this setup, the effects of changing the height of bundles, the radius of bundles, the spacing between bundles, and the bundles' number on the voltage-current characteristics are evaluated. Further, their impacts on the current density distribution on the ground plane are also assessed. For the same applied voltage, the results showed that the corona current decreases on increasing bundles' number and/or minimizing the spacing between bundles. Thus, the obtained results confirmed that the corona power losses can be optimized without increasing the conductor radius or its height above the ground. The obtained results by the proposed numerical approach (FDM-FMG) demonstrate its high accuracy rate where a strong matching with present and past experimental laboratory results are achieved.

2. Governing Equations and boundary conditions

To deal with the monopolar dc corona discharge problem, Poisson and current continuity equations are resolved as follows [1]:

$$\nabla^2 V = -\frac{\rho}{\varepsilon_o} \tag{1}$$

$$E = -\nabla V \tag{2}$$

$$j = \rho k E \tag{3}$$

$$\nabla . j = 0 \tag{4}$$

where V stands for the electric potential and ρ is the charge density. $\varepsilon_o$stands for the air permittivity, E is the electric field intensity, j represents the current density, and k is the ionic mobility. To solve such equations, the following boundary conditions are employed in the proposed algorithm (see Fig. 1):

1) The potential at the surface of the bundled wires is the applied potential (V).
2) The ground plate potential equals zero.
3) The space charge in the inter-electrode space is of monopolar type.
4) The ionization zone thickness on the bundled conductors is ignored.
5) The electric field around the conductor nearly equals the onset value.

For a more accurate estimation of the electric field around the conductor, the corona inception voltage V_{on} of line conductors for numerically assessing the corona environment of HVDC line conductors is determined according to the principle developed for the forming of the recurrence of negative corona current pulses in the near vicinity of the stressed conductor [45, 46]. The magnitude of the electric field at the surface of the coronating conductor E is not assumed constant at the onset value E_0 but it depends on how high the applied voltage is above the onset value, as follows:

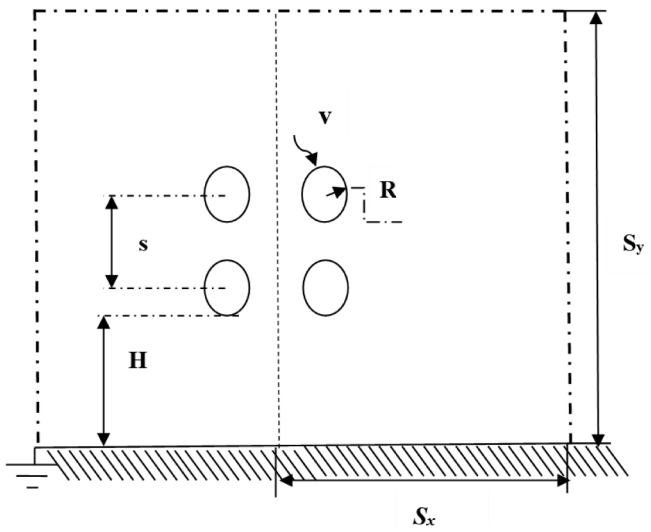

Fig. 1. Bundle four rectangular configuration.

$$E = E_{on} f_1\left(\frac{V}{V_{on}}\right) \tag{5}$$

in which

$$f_1 = 1.1339 - 0.1678\left(\frac{V}{V_{on}}\right) + 0.03\left(\frac{V}{V_{on}}\right)^2 \tag{6}$$

where V is the applied voltage, and empirically the onset field E_{on} can be formulated by [47]:

$$E_{on} = 30\, m\left(1 + \sqrt{\frac{9.06}{R}} \times 10^{-2}\right) \times 10^2 \tag{7}$$

where R and m are the radius of the bundle (m) and surface roughness factor, respectively. The current continuity formula is solved by the FDM. Combining Eqs. 3 and 4 results in:

$$\nabla . \rho k E = 0 \tag{8}$$

As the ion mobility is constant, the current continuity equation will give:

$$\frac{\rho^2}{\varepsilon_o} + E_x\frac{\Delta\rho}{\Delta x} + E_y\frac{\Delta\rho}{\Delta y} = 0 \tag{9}$$

Enforcing backward finite difference equations, Eq. 9 becomes

$$\frac{\rho_{m,n}{}^2}{\varepsilon_o} + E_x\left(\frac{\rho_{m,n} - \rho_{m,n-1}}{\Delta x}\right) + E_y\left(\frac{\rho_{m,n} - \rho_{m-1,n}}{\Delta y}\right) = 0 \tag{10}$$

Therefore, $\rho_{m,n}$ is estimated by solving the following formula [42]:

$$\left(\frac{\Delta x\, \Delta y}{\varepsilon_o}\right)\rho_{m,n}{}^2 + (\Delta x\, E_y + \Delta y\, E_x)\rho_{m,n} - (\Delta x\, E_y \rho_{m-1,n} + \Delta y\, E_x \rho_{m,n-1}) = 0 \tag{11}$$

in which E_x and E_y stand for the electric field intensity in X and Y

directions, respectively.$\Delta x$and Δystand for, respectively, the incremental distance in horizontal and vertical directions.

As the zone of the computational domain, Fig. 1, is indefinite, an artificial boundary extended in both directions should be implemented. At these boundaries, the outcome potential is supposed to be equal to the electrostatic potential [19]. Implementing the central finite difference method, the voltage at any point in the computational domain, Fig. 2 can be computed by:

$$v_{m,n} \cong \frac{1}{2\left(\Delta x^2+\Delta y^2\right)} \times \left(\Delta x^2\left(v_{m+1,\,n}+v_{m-1,\,n}\right)+\Delta y^2\left(v_{m,\,n+1}+v_{m,\,n-1}\right)+\frac{\Delta x^2\Delta y^2\rho_{m,n}}{\varepsilon_o}\right) \quad (12)$$

Extensible software has been developed in the Matlab program to model Poisson and continuity formulae on bundled conductors. The proposed method of solution can be summarized as below:

i Adjust the potential at the bundle conductors, and enter all the boundary conditions into the system of equations.
ii Evaluate the space charge-free field via the CSM.
iii At every point in the computational domain, the charge density is computed using Eq. 11 as an initial guess.
iv At every point in the computational domain, compute the potential using Eq. 12 by FDM and FMG as an iterative solver, until reaching a prescribed tolerance.
v Use the new values of potential calculated in the previous step, and recompute the charge density at every point in the computational domain again.

If the difference between each value of charge density at every point and its previous value is smaller than a prescribed error, then, the obtained potential and charge density values will be used to calculate the current density at the ground plane. Else, go to step (iv) and repeat the next steps.

3. Multigrid method

The Poisson equation takes too much time in the computational algorithm [36]. On finer grids, the traditional iterative techniques consume excessive time to converge to a certain solution. Therefore, the present algorithm proposes the multigrid technique to converge fast on finer computational grids. Among the different schemes of the multigrid technique, the present analysis uses the FMG with the finite difference technique [48]. FMG technique solves the coarsest domain and interpolates it to a finer domain where many V-cycles are performed. Fig. 3 demonstrates the flow chart that describes only one V–cycle. In the present study, to give the best performance in terms of the computational time, the number of pre-smoothing and post smoothing steps is 3 and 1 respectively, where $[I_{2h}^{h}]$ represents the standard full weighting operator and $[I_{h}^{2h}]$ represents an operator for the bilinear interpolation [42].

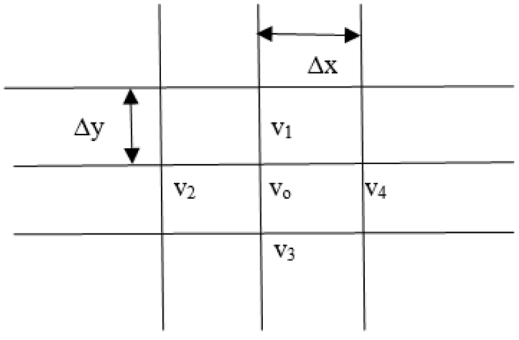

Fig. 2. Section of the intended grid.

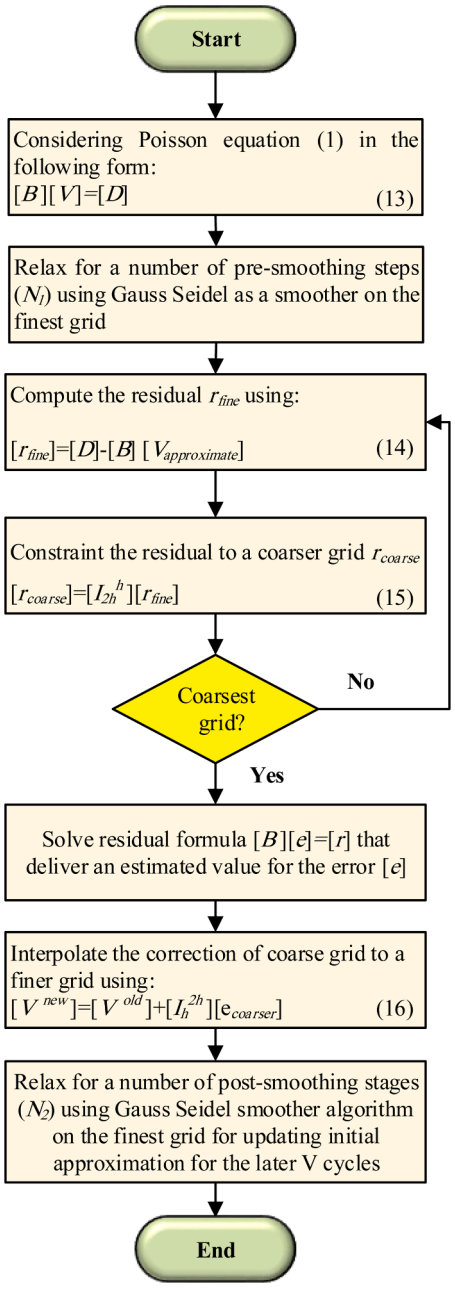

Fig. 3. Flow chart of one V-cycle.

4. Results and discussion

To emphasize the validity of the suggested method, (V/I) characteristics for Al-Hamouz's model for bundle two horizontal and bundle four rectangular transmission line (TL) designs are computed [38]. The radius of the wire (R) is 75×10^{-2} mm, located at a height (H) of 0.5 m above the ground plane and the spacing between bundles (s) is 0.04 m. The ion mobility and the roughness factor are taken 1.4×10^{-4} m^2/Vs and 1, respectively [38]. The FDM is performed here on a fine rectangular grid of (128 × 128) points, with an artificial boundary expanded for 2H in both directions. The overall program execution time is 0.6 sec, which reflects the importance of the FMG as a fast-convergent method.

An excellent congruence between the proposed technique and Al-

Hamouz et al. experimental results is achieved at different applied voltages, as shown in Fig. 4. This figure confirms that the increase in the bundles' number will minimize the corona current for the same applied voltage, resulting in the reduction of the corona power losses.

Fig. 5 compares the measured current densities at the grounded plate for single and bundle two horizontal HVDC transmission lines configuration introduced by Al-Hamouz model with the numerical results obtained here by the FDM [38]. Fig. 5 affirms the findings of Fig. 4, such that the bundle 2-horizontal configuration gives lower current density profiles at the ground plane than the single wire configuration at the same applied voltage. Also, the change in the bundles' number resulted in a different shape for the current density distribution. For bundle two horizontal HVDC transmission line, each wire contributes by a maximum value, so two maximum values are observed on the grounded plate, such that the area under each peak gives the corona current contributed by each sub-wire.

Also, the FDM is tested on a grid of (256 × 256) points, against the experimental data of the Abdel-Sattar model for a wire of diameter (2R) equals 1.6 mm located at height (H) of 7.67 cm above the ground surface and the spacing (s) between bundles is 1.5 cm in still air [36]. The proposed method computes the current density distribution over the grounded plane for bundle two horizontal and vertical configuration, and it agreed sufficiently with the laboratory results of Abdel-Sattar at different applied voltages, as demonstrated in Figs. 6 and 7. The corona onset fields for bundle two horizontal at 67.2 kV and 56 kV are 58.5 kV/cm and 59.85 kV/cm, respectively. For vertical configuration, the corona onset fields at 50.4 kV and 44.5 kV are 59 kV/cm and 60 kV/cm, respectively. The ion mobility and the roughness factor are taken 1.4×10^{-4} m^2/Vs and 1, respectively.

Referring to Fig. 7, the experimental data for Bundle 2 horizontal is used to compare the proposed FDM-FMG with traditional techniques such as the modified finite element method introduced by Al Hamouz et al. [38].

Fig. 8 demonstrates the percentage error by FDM-FMG and the modified finite element method introduced by Al Hamouz [38] for different spacing on the grounded plate. As seen from the figure, the maximum error by FDM-FMG is 12% and for FEM is 28%. This reflects the importance of using FMG as an iterative solver to work on fine computational domains without suffering from high computational time. FDM with the help of FMG decreases the truncation error by working on fine domains. The above observations show that the use of the FDM integrated with FMG on fine domains is superior over FEM.

Fig. 9 describes the calculated current density profile by the FDM for the bundle-4 diamond system with wire diameter 0.85 mm compared to the experimental work of Abdel-Sattar at different applied voltages, and a strong agreement is reached [36]. The corona onset fields at 54 kV and 44 kV are 61.5 kV/cm and 62.8 kV/cm, respectively. It was noted that the corona current contributed from the upper sub-wires is very small to be observed at the ground plate, and so one peak value is detected.

Figs. 6, 7, and 9 show that as the applied voltage increases, the total current reached the ground plate rises as well as the current density, resulting in higher corona losses.

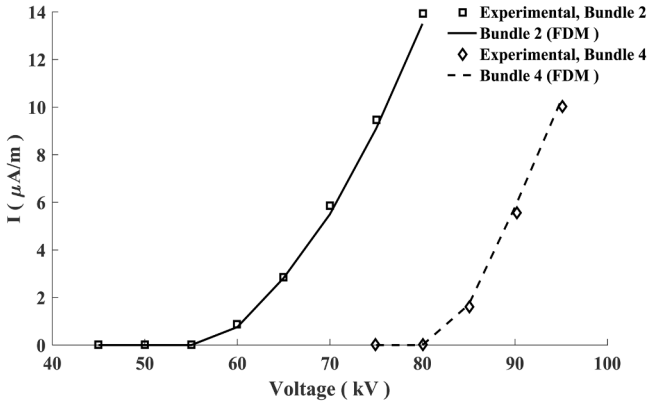

Fig. 4. Effect of the variation of bundles' number on the voltage current characteristics by the experimental results in [38] and the proposed method.

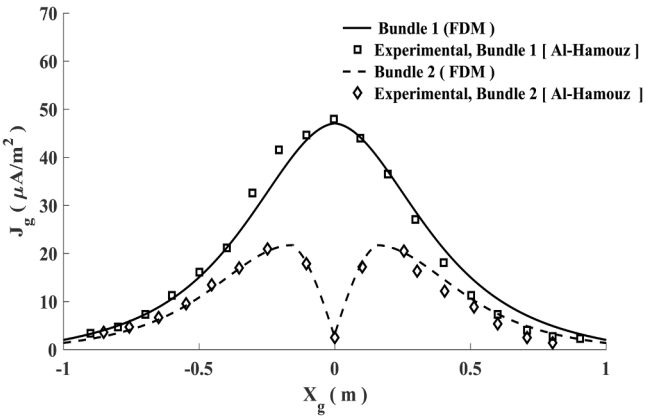

Fig. 5. Current density distribution along the ground plane for single and bundle two horizontal conductors, H = 0.59 m, s = 0.02 m, V = 100 kV by the experimental results in [38] and the proposed method.

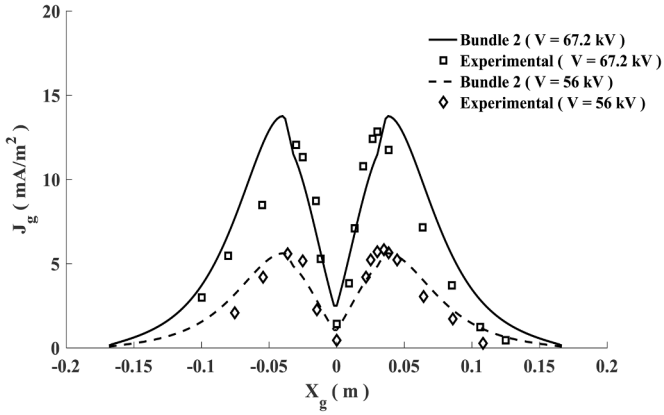

Fig. 6. Current density distribution on ground plate for bundle 2 model, horizontal configuration by the experimental results in [36] and the proposed method.

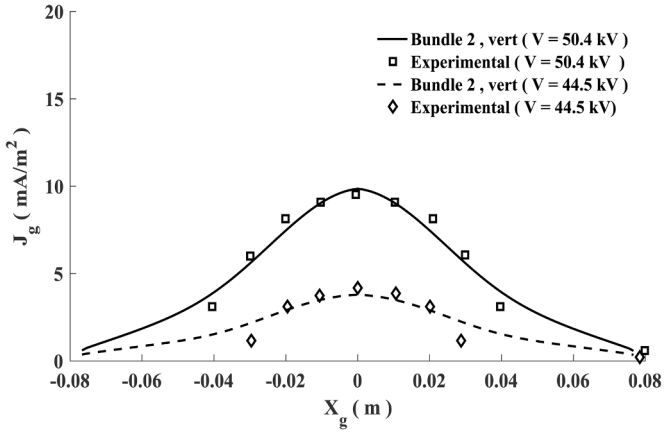

Fig. 7. Current density distribution on ground plate for bundle 2 model, vertical configuration by the experimental results in [36] and the proposed method.

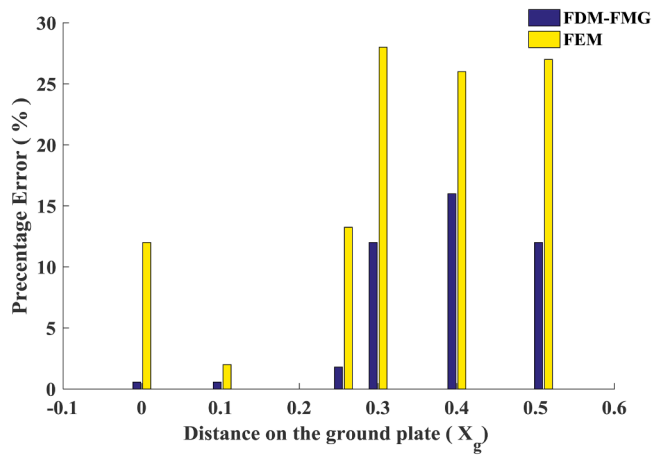

Fig. 8. Percentage error by FDM-FMG and the modified finite element method introduced by Al Hamouz et al. [38] for different spacing on the grounded plate.

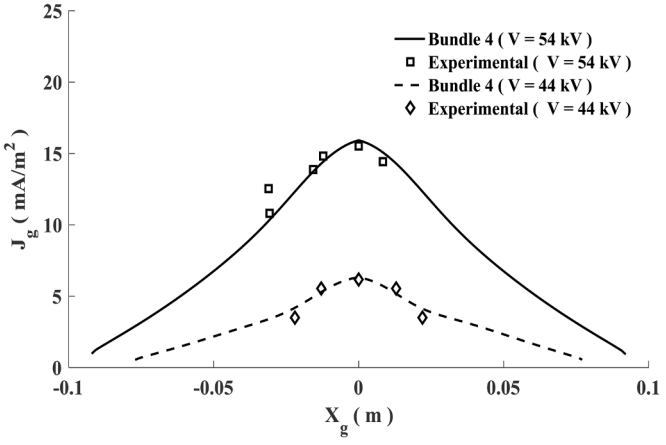

Fig. 9. Current density distribution on ground plate for bundle 4 model, diamond configuration by the experimental results in [36] and the proposed method.

An experimental setup was constructed to validate the proposed method of analysis (see Fig. 10). The simulated HVDC bundled transmission line is hanged at a certain height above the grounded aluminum plate. The dimensions of the grounded aluminum plate are 0.98 × 1.9 m^2, and its thickness is 1 mm. The aluminum plate is divided into 46 strips (each of 1.9 × 0.02 m^2) where the strips are isolated by 0.1 cm apart, and each one is connected to the ground through a micrometer device. In order to prevent the corona discharge from the ends of the bundles, two spherical caps are implemented in the design. The setup is designed in a way to study the variation of different parameters like the number, height, and radius of bundles. A high voltage DC source (Hipotronics, Model 800PL-10MA series) has been used to energize the HVDC bundled transmission line to a maximum of 80 kV and 10 mA.

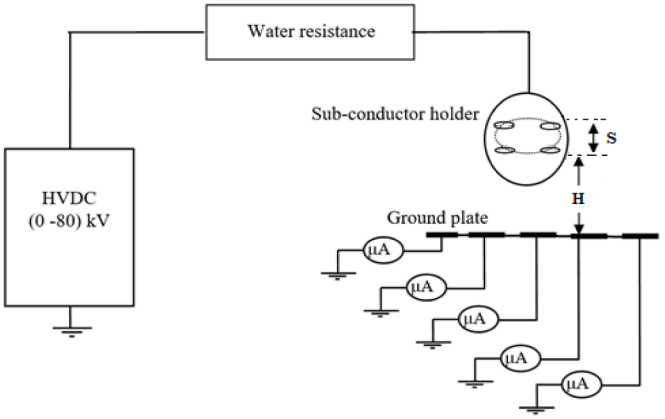

Fig. 10. Experimental setup.

The FDM with the help of the FMG solver is formulated on (256 × 256) grid points, and the overall program execution time is 10 sec to reach a convergence of 10^{-8} %, and the numerical results obtained are compared with the experimental results implemented by the setup shown in Fig. 10, which complies with IEEE standard (539-2005). The grounding impedance connected to the experimental setup mentioned in Fig. 10 is measured using MEGGER DET5/3R earth tester and its value equals 2.3 Ω. In the HV laboratory, we follow the IEEE standard (81-2012) for measuring the earth resistivity, ground impedance, and earth surface potentials of a ground system.

The experimental setup is designed to validate the proposed numerical method (FDM-FMG). For this purpose, the horizontal and vertical two bundles are implemented such that the wire diameter is 1 mm at a height of 20.25 cm above the ground plate, and the spacing between bundles is 15 mm (s =15 mm). The ion mobility and the roughness factor are taken 1.4 × 10^{-4} m^2/Vs and 1, respectively. Fig. 11.a illustrates the voltage-current characteristics of the bundle's two horizontal and vertical designs. It was found that, at the same applied voltage, the corona current for the vertical configuration is more than the horizontal one.

Fig. 11.b demonstrates the current density distribution along with the ground plate for the bundle two horizontal and vertical transmission

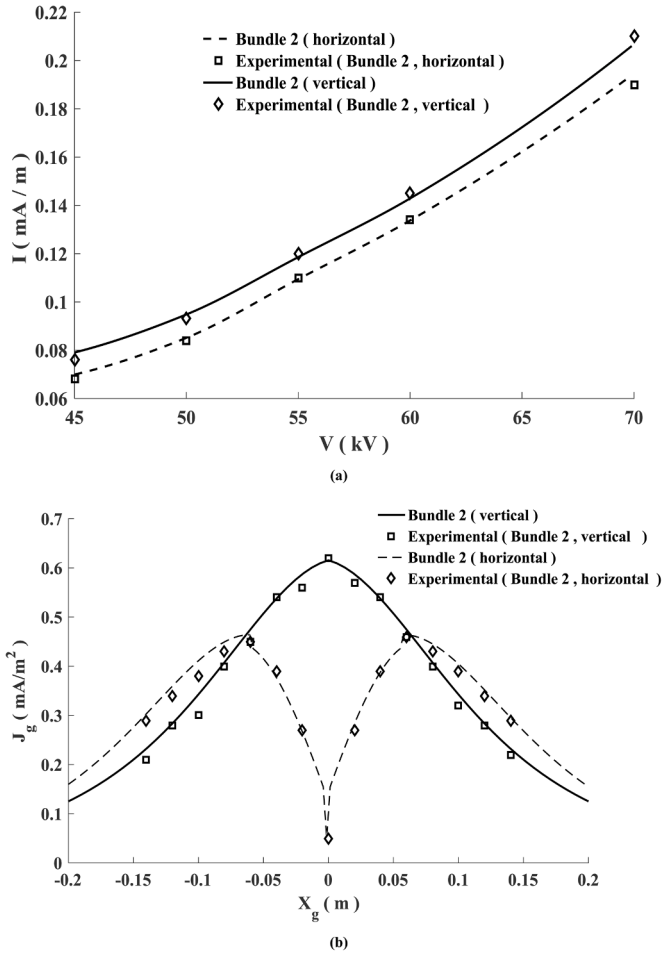

Fig. 11. Bundled two horizontal and vertical configurations; **a)** V-I characteristics, **b)** Current density distribution on ground plate.

line design at an applied voltage of 55 kV. This latter figure declares the results of Fig. 11.a such that the current density for the vertical bundle is higher than that of the horizontal bundle, which will lead to higher corona losses. It is important to mention that not only the magnitude is different, but also the shape of the current density profile is completely different. In the case of vertical bundles, the lower conductor contributes most to the corona current, and hence one peak value is found, whereas in the horizontal configuration, the two conductors almost contribute equally and hence two peak values are observed. The results are confirmed by the findings of Abdel Sattar [36]. The corona onset fields for bundle two horizontal and vertical at 55 kV are 68.24 kV/cm and 66 kV/cm, respectively. The ion mobility and the roughness factor are taken 1.4×10^{-4} m^2/Vs and 1, respectively.

Also, the experimental setup, Fig. 10, is implemented to show the effectiveness of altering the wire radius on the voltage-current characteristics and the current density distributions on the grounded plate for horizontal two bundle configuration. Fig. 12.a shows the voltage-current characteristics for the bundle two horizontal configuration for different wire radii. It was observed that the decrease in the radius of the bundle will increase the corona current at the similarly applied voltage. The corona current decreases by 14 % when the wire radius increases from 0.35 mm to 0.75 mm at an applied voltage of 70 kV.

Fig. 12.b demonstrates the current density distribution over the ground plate for the bundle-2 horizontal transmission line configuration for different wire radii at an applied voltage of 70 kV. It is illustrated that as the bundle radius increases, the current density received by the ground plate decreases resulting in lower corona power losses. Indeed, increasing the wire radius increases the corona onset voltage of the wire resulting in a lower corona current and hence lower current density at the ground plate for the same applied voltage. When the wire radius increases from 0.35 mm to 0.75 mm, the maximum current density decreases by 16 %. The present method matched well with the laboratory results. The corona onset fields at 70 kV are 71.3 kV/cm and 58.6 kV/cm for a wire radius of 0.35 mm and 0.75 mm, respectively.

The impact of the bundle height variation over the grounded plate on the voltage-current characteristics and the current density distributions on the grounded plate for horizontal two bundle configuration is assessed. Fig. 13.a describes the voltage-current characteristics for the bundle two horizontal configuration for different bundle height (H). It was found that the increase in the height of the bundle, decreases the corona current at the same applied voltage. This is explained by the that as the wire height increases, the corona onset voltage of the wire increases resulting in a lower corona current received by the grounded plate. The corona current decreases by 91% when the wire height increases from 9.25 to 20.25 cm at an applied voltage of 70 kV.

Fig. 13.b explains the current density distribution over the ground plate for the bundle-2 horizontal transmission line configuration for different bundle height at an applied voltage of 50 kV. As the bundle height over the grounded plate increases, the current density received by the ground plate reduces resulting in lower corona losses. When the wire height increases from 9.25 cm to 20.25 cm, the maximum current density decreases by 92%, and the current density profile becomes broader. It is worth mentioning that the change in the bundle height is more significant than the change in the wire radius with respect to the value of the corona onset voltage and hence on the corona power losses.

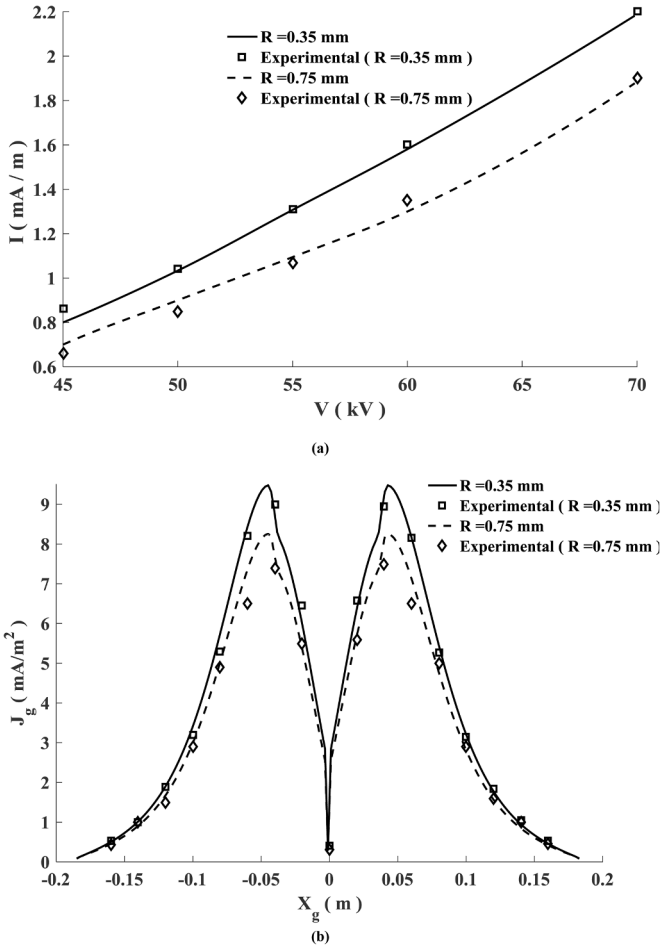

Fig. 12. Effect of variation of bundle radius(H = 9.25cm, s =15 mm); **a)**V-I characteristics, **b)** Current density distribution on ground plate.

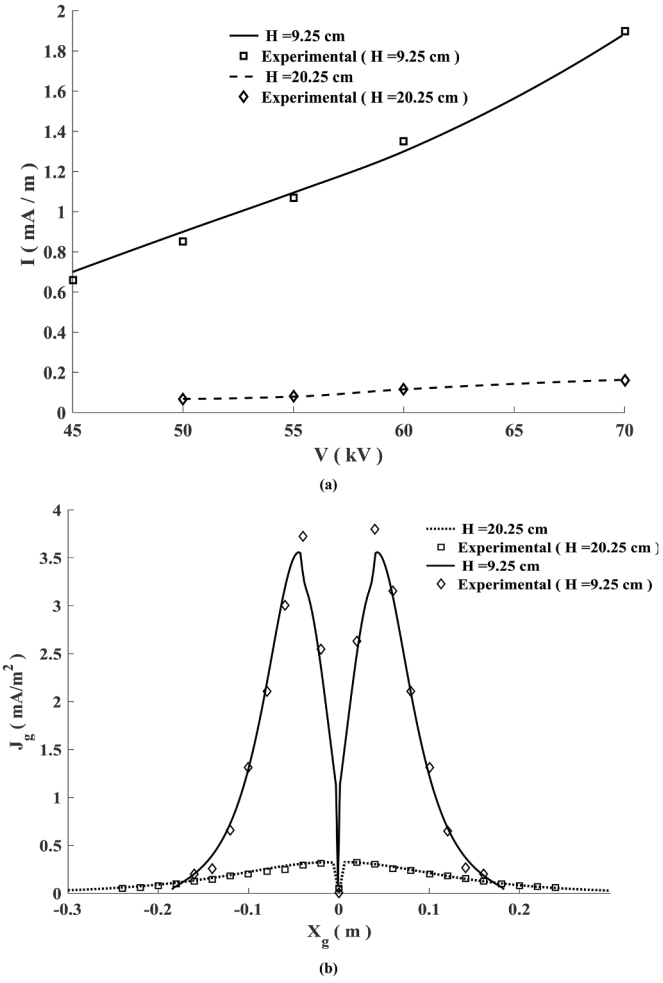

Fig. 13. Effect of variation of bundle Height(R =0.75mm, s=15 mm); **a)**V-I characteristics, **b)**Current density distribution on ground plate.

The corona onset field at 50 kV is 61.9 kV/cm for a wire height of 20.25 cm.

Also, the influence of varying the spacing between the bundles on the voltage-current characteristics and the current density distributions on the grounded plate for horizontal two bundle configuration is studied. Fig. 14.a shows the voltage-current characteristics for the bundle two horizontal configuration for different spacing between bundles. When the bundle spacing increases, the corona onset voltage of the wire reduces, which in turn increases the corona current for the same applied voltage. The corona current increases by 7% when the spacing increases from 15 mm to 30 mm at an applied voltage of 70 kV.

Fig. 14.b demonstrates the current density distribution over the ground plate for the bundle-2 horizontal transmission line configuration for different spacing between bundles at an applied voltage of 60 kV. As the spacing between bundles increases, the current density received by the ground plate increases resulting in higher corona power losses. When the spacing increases from 15 mm to 30 mm, the maximum current density increases by 8%. It must be noticed that the bundle spacing variation is not significant regarding the value of the corona onset voltage and hence on the corona power losses. The corona onset field at 60 kV is 72 kV/cm for bundle spacings 30 mm.

Fig. 15.a shows the percentage error between the numerical method and the experimental results at different applied voltage. Interestingly, the maximum error has not exceeded 5% at s = 30 mm and 4.5% for s=15 mm. Further, the percentage error is evaluated at an applied voltage of 60 kV for different distances on the ground plate (see Fig. 15.

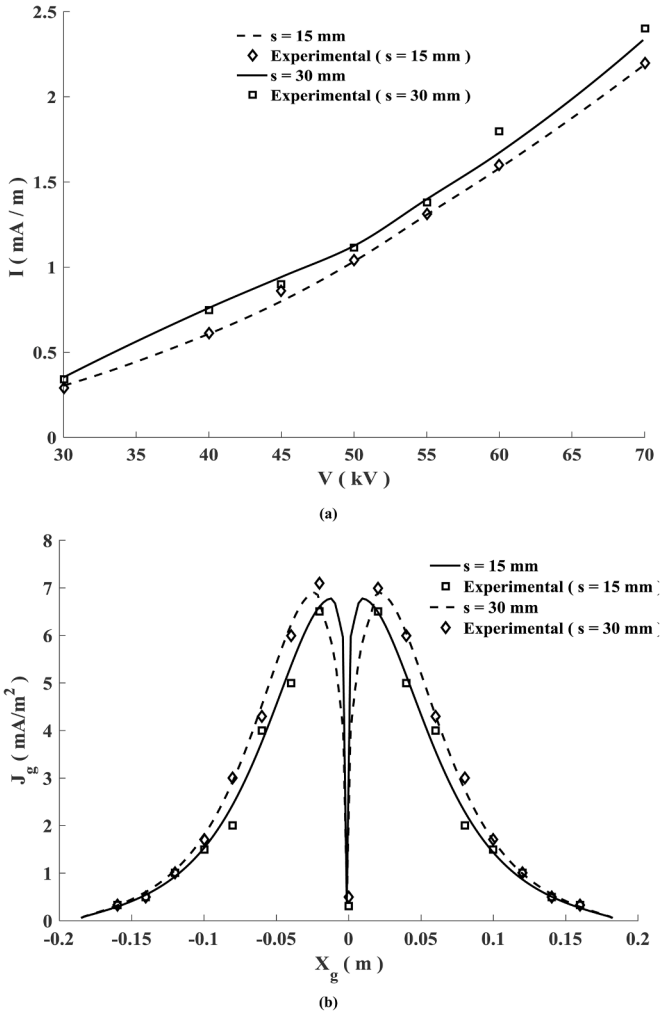

Fig. 14. Effect of variation of bundle spacing (R=0.35 mm, H=9.25 cm); **a)**V-I characteristics, **b)**Current density distribution on ground plate.

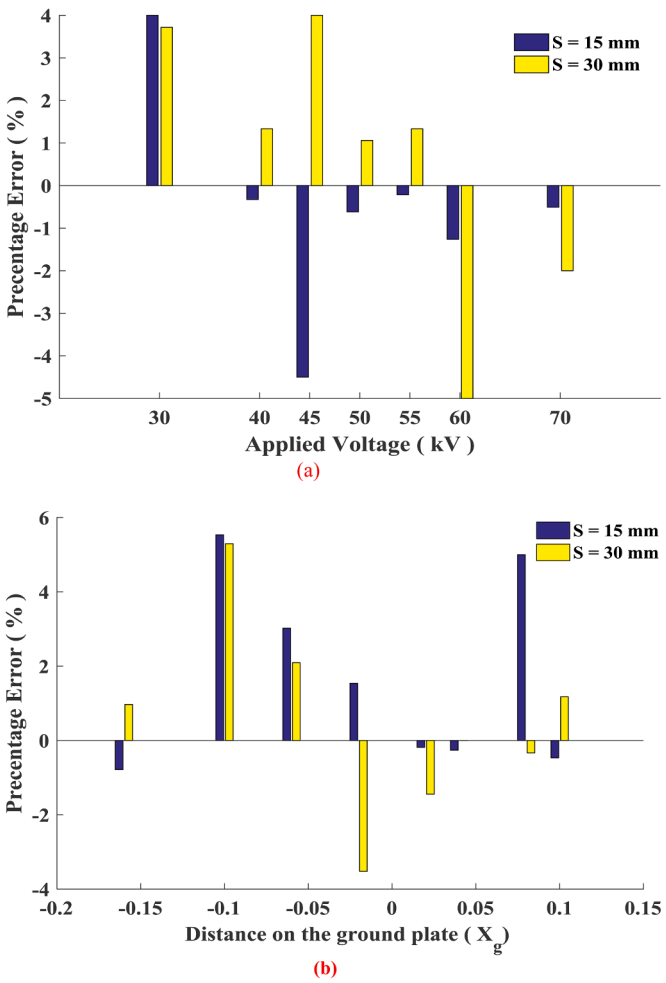

Fig. 15. Percentage error between the numerical method and the experimental results with the variation of bundle spacing; **a)**for different applied voltage, **b)** for different distances on the ground plate.

b). As noticed, the maximum error does not exceed 5.2% at s=30 mm and 5.5% for s = 15 mm. Generally, the maximum error in both cases does not exceed 10%, which is acceptable for numerical methods that well-matched with the experimental results of current density distribution as indicated in Fig. 14.

Finally, the influence of changing the bundles' number on the V/I characteristics and current density profiles on the ground plate is studied. Fig. 16.a illustrates the V/I characteristics for the single, horizontal two bundle, and rectangular four bundle configurations. It was pointed out that by increasing the bundles' number, the onset voltage of the wire increases which in turn decreases the corona current at the same applied voltage. The corona current decreases by 78% when using rectangular bundle-4 instead of the single wire configuration at an applied voltage of 70 kV.

For the above-mentioned configurations, Fig. 16.b displays the current density distribution over the ground plate at 70 kV. Through increasing the bundles' number, it was noted that the current density received by the ground plate decreases resulting in lower corona power losses. The maximum current density for the single wire transmission line decreases by 63% when it is replaced by a rectangular bundle-4. Therefore, the change in the number of bundles greatly affects the corona onset voltage and hence the corona power losses, without the need of increasing the height or using larger conductor diameter defined by the transmission-line current capacity, and this is the main aim of bundling in the design of HVDC transmission lines.

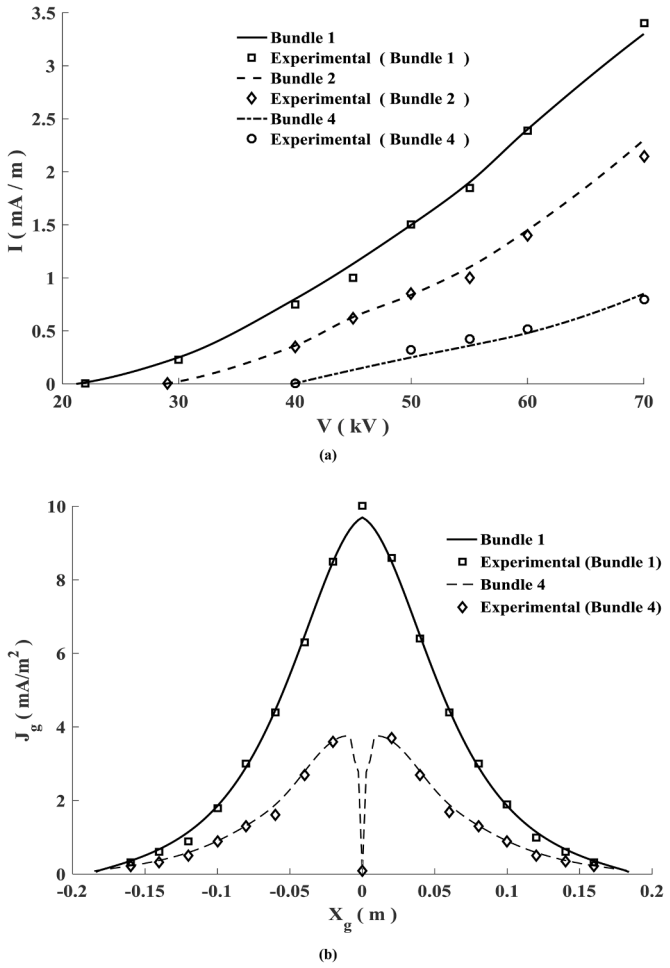

Fig. 16. Effect of variation of number of bundles (R =0.5 mm, H= 9.25 cm, s = 15 mm); **a)**V-I characteristics, **b)**Current density distribution on ground plate.

5. Conclusions

In this paper, an intensive measurement and analysis of monopolar ionized fields in bundled HVDC conductors have been introduced using the FDM based on the FMG. The use of the FMG decreases the truncation error for the finite difference approximations by working on fine computational domains without suffering from the high computational time. Based on that, the FDM integrated with FMG is tested against the finite element method and the latter is completely transcendent owing to the numerical outcomes with respect to the experimental values. The maximum error in FDM-FMG does not exceed 10%. The following other conclusions are noticed:

- Monopolar ionized fields in HVDC bundled conductors have been assessed using FDM combined with the FMG solver.
- The FMG is time-efficient, as it converges fast on the finer computational domains to reach a prescribed tolerance.
- The overall program execution time is 10 seconds to converge to a prescribed tolerance on a grid of (256 × 256) points.
- The numerical outcomes by the present analysis concurred well with the past and present laboratory results.

Credit Author Statement

Mohamed A. Abouelatta: Conceptualization, Experimental setup, Data curation, Writing - review & editing. **Sayed A. Ward:** Investigation, Visualization, Supervision. **Ahmad M. Sayed:** Software, Validation, Experimental setup, Writing - original draft. **Karar Mahmoud:** Software, Resources, Formal analysis. **Matti Lehtonen:** Writing - review & editing, Supervision, Funding acquisition. **M. M. F. Darwish:** Conceptualization, Methodology, Investigation, Writing - original draft.

Declaration of Competing interest

The authors declare that they have no known competing financial interests or personal relationships that could have appeared to influence the work reported in this paper.

Acknowledgement

This work was supported by the high voltage laboratory Faculty of engineering at Shoubra Benha University, Egypt and also by Department of Electrical Engineering and Automation, School of Electrical Engineering, Aalto University, Espoo, Finland.

References

[1] Y. Tian, X. Huang, W. Tian, Hybrid method for calculation of ion-flow fields of HVDC transmission lines, IEEE Trans. Dielectri. Electr. Insulat. 23 (5) (2016) 2830–2839.
[2] J. Qiao, et al., Method of local characteristics for calculating electric field and ion current of HVDC transmission lines with transverse wind, IET Gener. Transmis. Distrib. 11 (4) (2017) 1055–1062.
[3] P.S. Maruvada, Electric field and ion current environment of HVDC transmission lines: Comparison of calculations and measurements, IEEE Trans. Power Deliv. 27 (1) (2012) 401–410.
[4] E.I. Bousiou, P.N. Mikropoulos, V.N. Zagkanas, Corona Inception Field Of Typical Overhead Line Conductors Under Variable Atmospheric Conditions, 178, Electric Power Systems Research, 2020, 106032.
[5] X. Zhou, et al., Shielding effect of HVAC transmission lines on the ion-flow field of HVDC transmission lines, IEEE Trans. Power Deliv. 28 (2) (2013) 1094–1102.
[6] Y.M. Li, W. Li, Simple algorithm for calculating the total electric field of high-voltage direct current transmission lines, IET Gener. Transmis. Distrib. 8 (1) (2014) 187–192.
[7] M. Abdel-Salam, M.T. El-Mohandes, S.K. El-deen, A simplified method for quick calculation of Corona I–V characteristics of unipolar transmission-line configurations, IEEE Trans. Plasma Sci. 48 (3) (2020) 631–642.
[8] C.K. Arruda, A.C. Lima, Corona modeling in HVDC Transmission Lines Based On A Modified Particle-In-Cell Approach, 125, Electric Power Systems Research, 2015, pp. 91–99.
[9] Z.M. Al-Hamouz, A hybrid computational technique for the estimation of corona power loss associated with bundled transmission lines, Electr. Power Syst. Res. 50 (1) (1999) 65–70.
[10] Y. Jiang, H. Liu, Z. Liang, Q. Li, S. Ma, J. Cheng, Calculation of electric field under HVDC transmission lines with bundle conductors, in: Proceedings of the IEEE 7th International Conference on Computer Science and Network Technology (ICCSNT), Dalian, China, 2019, pp. 83–86.
[11] M. Abdel-Salam, M.T. El-Mohandes, S.K. El-deen, Analysis of corona discharge in wire-cylinder ESP with and without particle loading, IEEE Trans. Dielectri. Electr. Insulat. 23 (5) (2016) 2607–2616.
[12] G. Huang, J. Ruan, Z. Du, C. Zhao, Highly Stable Upwind FEM for solving ionized field of HVDC transmission line, IEEE Trans. Magn. 48 (2) (2012) 719–722.
[13] N.G. Trinh, P.S. Maruvada, B. Poirier, A comparative study of the corona performance of conductor bundles for 1200 kV transmission lines, IEEE Trans. Power Apparat. Syst. PAS-93 (3) (1974) 940–949.
[14] F. Xiao, B. Zhang and Y. Deng, "Experimental study on impulse corona characteristics of HVDC conductors with space charges," in Proceedings of the IEEE Transactions Power Delivery, doi: 10.1109/TPWRD.2020.3013642.
[15] M. Elsisi, K. Mahmoud, M. Lehtonen, M.M.F. Darwish, Reliable industry 4.0 based on machine learning and IoT for analyzing, monitoring, and securing smart meters, Sensors 21 (2021) 487.
[16] A.J. Otto, H.C. Reader, HVDC corona space charge modeling and measurement, IEEE Trans. Power Deliv. 26 (4) (2011) 2630–2637.
[17] J.L. Davis, J.F. Hoburg, HVDC transmission line computations using finite element and characteristics method, J. Electrost. 18 (1) (1986) 1–22.
[18] M. Abdel-Salam, M. Farghally, S. Abdel-Sattar, Finite element solution of monopolar corona equation, IEEE Trans. Electr. Insulat. EI-18 (2) (1983) 110–119.
[19] W. Janischewskyj, G. Cela, Finite element solution for electric fields of coronating DC transmission lines, IEEE Trans. Power Apparat. Syst. PAS-98 (3) (1979) 1000–1012.
[20] T. Takuma, T. Ikeda, T. Kawamoto, Calculation of ion flow fields of HVDC transmission lines by the finite element method, IEEE Trans. Power Apparat. Syst. PAS-100 (12) (1981) 4802–4810.
[21] M. Abdel-Salam, Z. Al-Hamouz, Finite-element analysis of monopolar ionized fields including ion diffusion, J. Phys. D: Appl. Phys. 26 (12) (1993) 2202.

[22] M. Abdel-Salam, Z. Al-Hamouz, A. Mufti, Open-boundary finite-element analysis of ionized field around monopolar transmission lines, J. Electrost. 39 (2) (1997) 129–144.
[23] Z. Al-Hamouz, Finite element computation of corona around monopolar transmission lines, Electr. Power Syst. Res. 48 (1) (1998) 57–63.
[24] T. Lu, et al., Analysis of the ionized field under HVDC transmission lines in the presence of wind based on upstream finite element method, IEEE Trans. Magn. 46 (8) (2010) 2939–2942.
[25] H. Nouri, et al., Numerical analyze of corona discharge on HVDC transmission lines. World academy of science, engineering and technology, Int. J. Electr. Comput. Energ. Electron. Commun. Eng. 9 (6) (2015) 627–631.
[26] M. Yu, E. Kuffel, J. Poltz, A new algorithm for calculating HVDC corona with the presence of wind, IEEE Trans. Magn. 28 (5) (1992) 2802–2804.
[27] M. Yu, E. Kuffel, A new algorithm for evaluating the fields associated with HVDC power transmission lines in the presence of corona and strong wind, IEEE Trans. Magn. 29 (2) (1993) 1985–1988.
[28] D. Rabah, C. Abdelghani, H. Abdelchafik, Efficiency of some optimisation approaches with the charge simulation method for calculating the electric field under extra high voltage power lines, IET Gener. Transmis. Distrib. 11 (17) (2017) 4167–4174.
[29] M.N. Horenstein, Computation of corona space charge, electric field, and VI characteristic using equipotential charge shells, IEEE Trans. Ind. Appl. IA-20 (6) (1984) 1607–1612.
[30] M. Abdel-Salam, S. Abdel-Sattar, Calculation of corona VI characteristics of monopolar bundles using the charge simulation method, IEEE Trans. Electr. Insulat. 24 (4) (1989) 669–679.
[31] Z. Li, et al., Numerical calculations of monopolar corona from the bare bundle conductors of HVDC transmission lines, IEEE Trans. Power Deliv. 24 (3) (2009) 1579–1585.
[32] M.P. Sarma, W. Janischewskyj, Corona loss characteristics of practical HVDC transmission lines, part I: unipolar lines, IEEE Trans. Power Apparat. Syst. PAS-89 (5) (1970) 860–867.
[33] M. Abdel-Salam, M. Farghaly, S. Abdel-Sattar, Monopolar corona on bundle conductors, IEEE Trans. Power Apparat. Syst. PAS-101 (10) (1982) 4079–4089.
[34] M. Abdel-Salam, M. Farghaly, S. Abdel-Sattar, DC corona discharge on monopolar bundle wires, Acta Physica Hungarica 54 (3-4) (1983) 313.
[35] S. Abdel-Sattar, Numerical method to calculate corona profiles at ground level and underneath monopolar lines as influenced by wind, IEEE Trans. Electr. Insulat. EI-21 (2) (1986) 205–211.
[36] S.E. Abdel-Sattar, Monopolar corona on bundle wires as influenced by wind, IEEE Trans. Ind. Appl. IA-23 (6) (1987) 984–989.
[37] Y. Sunaga, Y. Sawada, Method of calculating ionized field of HVDC transmission lines and analysis of space charge effects on RI, IEEE Trans. Power Apparat. Syst. PAS-99 (2) (1980) 605–615.
[38] Z. Al-Hamouz, M. Abdel-Salam, Finite-element solution of monopolar corona on bundle conductors, IEEE Trans. Ind. Appl. 35 (2) (1999) 380–386.
[39] W.L. Briggs, V.E. Henson, S.F. McCormick, A multigrid tutorial, Soci. Ind. Appl. Math. (2000).
[40] T. Guillet, R. Teyssier, A simple multigrid scheme for solving the Poisson equation with arbitrary domain boundaries, J. Comput. Phys. 230 (12) (2011) 4756–4771.
[41] F. Gibou, et al., A second-order-accurate symmetric discretization of the Poisson equation on irregular domains, J. Comput. Phys. 176 (1) (2002) 205–227.
[42] A.M. Omar, M.A. Abouelatta, Fast corona discharge solver for precipitators using multi-grid methods on fine grids, IET Sci. Meas. Technol. 13 (3) (2019) 453–460.
[43] Y. Liu, F. Gao, L. Zhang, Multigrid method with adaptive gauss-seidel smoother for solving poisson equations, in: Proceedings of the 2nd International Conference on Information Engineering and Computer Science, Wuhan, 2010, pp. 1–3.
[44] M.A. Abouelatta, A.M. Omar, S. Ward, Optimal Grid Size For Precipitators Using Finite Difference Method Based On Full Multi-Grid Method, 189, Electric Power Systems Research, 2020, 106575.
[45] Mohamed Anwar Abouelatta, Badawi Said Mohamed, Omar Ahmed Mohamed, Negative corona inception voltage determination in the three-electrode system, in: Proceedings of the Twentieth International Middle East Power Systems Conference (MEPCON), IEEE, 2018.
[46] M.M. El-Bahy, S.A. Ward, R. Morsi, M. Badawi, Onset voltage of a particle initiated negative corona in a co-axial cylindrical configuration, J. Phys. D: Appl. Phys. 46 (2013) 1–10.
[47] F. Peek, Determination Phenomina in High Voltage Engineering, McGraw-Hill, New York, 1929, pp. 52–80.
[48] M.A. Abouelatta, S.A. Ward, Ahmad M. Sayed, K. Mahmoud, M. Lehtonen, M.M. F. Darwish, Fast corona discharge assessment using FDM integrated with full multigrid method in HVDC transmission lines considering wind impact, IEEE Access 8 (2020) 225872–225883.